Theoretical Description of the Role of Halides, Silver, and Surfactants on the Structure of Gold Nanorods

Neyvis Almora-Barrios, Gerard Novell-Leruth, Peter Whiting, Luis M. Liz-Marzán, Núria López

corresponding author: nlopez@iciq.es

Theoretical description of the role of halides, silver, and surfactants on the structure of gold nanorods

Neyvis Almora-Barrios, [†] *Gerard Novell-Leruth,* [†] *Peter Whiting,* [†] *Luis M. Liz-Marzán,* [‡,] *Núria López* *[†]*

† Institute of Chemical Research of Catalonia, ICIQ, Av. Països Catalans, 16, 43007, Tarragona, Spain

‡ BioNanoPlasmonics Laboratory, CIC biomaGUNE, Paseo de Miramón 182, 20009, Donostia - San Sebastián, Spain

Ikerbasque, Basque Foundation for Science, Bilbao, Spain

Gold nanorods · surfactants · halides · DFT · symmetry breaking

ABSTRACT

Density Functional Theory simulations including dispersion provide an atomistic description of the role of different compounds in the synthesis of gold-nanorods. Anisotropy is caused by the formation of a complex between the surfactant, bromine, and silver that preferentially adsorbs on some facets of the seeds, blocking them from further growth. In turn, the nanorod structure is driven by the perferential adsorption of the surfactant, which induces the appearance of open {520} lateral facets.

Understanding synthesis-structure relationships constitutes a major challenge in the study of materials science and catalysis. Such relationships could abridge the usually cumbersome synthetic procedures. However, complex synthetic conditions with multiple parameters and computational difficulties in coping with the large dimensions and long timescales necessary for worthwhile simulations mean that sufficiently detailed studies on synthesis mechanisms are still scarce. One of the most revealing sets of experiments with a large body of data regarding the different architectures of nanoparticles is the surfactant driven growth of gold nanocrystals. By slightly modifying the growth conditions different architectures can be reached, opening the way toward a myriad of applications in sensing and plasmonics.[1,2] Among such a variety of shapes, nanorods are definitely the most popular choice.

Nanorods are commonly prepared by seeded growth on 1-2 nm Au seeds, which are prepared by reduction of $HAuCl_4$ with $NaBH_4$ in a solution with hexadecyltrimethylammomium bromide (CTAB). A growth solution containing $HAuCl_4$ and a milder reductant, usually ascorbic acid, is then added to the seed solution. Importantly, silver nitrate and CTAB are also present in the growth solution and are believed to be crucial to induce nanorod growth.[3] In fact, the final aspect ratio and dimensions of the rods can be tuned through small variations of silver nitrate concentration.[4-7] Elemental analysis has shown that about 9% of the nanorod is actually Ag, which means between 2.5 and 4.3% of the surface atoms.[3] X-ray photoelectron spectroscopy (XPS) has been used to confirm adsorption of Br and both Au-Br and Ag-Br interactions,[8] and recent surface-assisted laser desorption/ionization time-of-flight mass spectrometry has identified adsorbed [Br-Ag-Br]$^-$ ions on the gold surfaces.[9] Several experimental evidences have also been reported that support the organization of CTAB as a surfactant bilayer covering the surface of the

nanorods.[10] The crystalline structure of Au nanorods has been analyzed in detail and structural features have been described, though there has been considerable debate in the literature. Wang et al.[11] indicated an octagonal cross-section in which alternating {100} and {110} planes form the lateral surfaces, with an angle between planes of 135º, and tips containing {110} and {111} facets. Recent reports based on more sophisticated electron microscopy techniques claim that the lateral facets actually comprise rather open {1250}[12] or {520} crystal planes.[13] However, this issue is not fully settled, as atomic-resolution electron tomography has revealed that {520} facets may coexist with {100}/{110} facets, which can be influenced by the choice of surfactant.[14] It should be noted that {520} and {1250} planes are nearly equivalent as the former is formed by {100}/{110} terraces and steps, and in the latter a central terrace is present.

All the ingredients, including Ag^+ ions, seem to be crucial for the selective formation of nanorods. Recently, Murphy et al.[3] have summarized the three different mechanisms proposed to account for the aspect ratio control observed by Ag: (i) deposition of a submonolayer of Ag on the lateral AuNR faces (silver under-potential deposition); (ii) the synergic behaviour of an unspecified CTA-Br-Ag^+ complex as face-specific capping agent; and (iii) the Ag and Br modulated solf-templating effect of the micelles (the ions inducing the spherical to cylindrical transition). The evolving nanoparticle morphology identified by stabilizing different growth stages through thiol adsorption[15] has shown that the seed rapidly elongates, followed by widening, generating {110} and {100} surfaces that ultimately evolve into {520} facets.

All these experiments call for the use of reliable theoretical methods. The surface energy, adsorption energy, and interaction sites can be obtained from molecular dynamics simulations in solution. These methods have been employed with success to study the interaction of large molecules or ionic liquids on gold.[16-19] However, they require experimental data as the employed

potentials that are fitted to some observables. Alternatively, first principles methods do not require this input. The interactions including polarization and charge transfer do not need to be pre-empted[20] and had large success in the field of chemical activity,[20,21] not only being able to reproduce data but also as a predictive tool. Unfortunately, Density Functional Theory, DFT, methods cannot easily consider the role of the solvent when applied to surfaces. In our case however, the interaction of water with these gold surfaces is quite weak. Therefore, mechanisms (*i*) and (*ii*) as described in the previous paragraph can be safely analyzed by DFT. To this end we: (*i*) analyzed the surface energy of different facets; (*ii*) described the effect of halides; and (*iii*) investigated the potential role of Ag on the thermodynamics of the growth process.
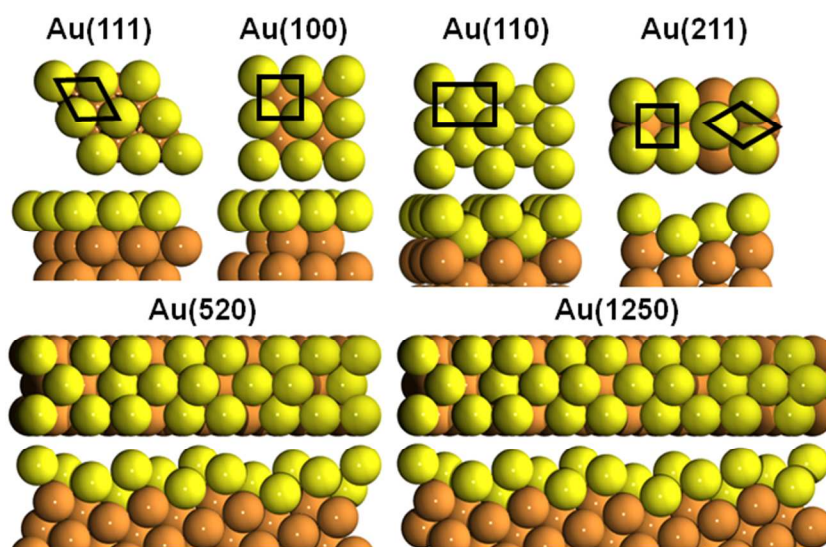

Figure 1. Top and lateral views are presented for: Au(111), (100), (110), stepped (211), (520) and (1250). Different facets that comprise open surfaces are marked by black lines for (111), (100), (110), and (211) planes.

Calculations were performed with the VASP code.[22-24] The methodology follows that of Remediakis *et al.*[25] where the surface energies have been computed through the PBE

functional.[26] For the interaction energies of large molecules a DFT-D2 approach[27,28] to account for dispersion terms has been employed with the parameters developed by Tatchenko and coworkers.[29] Inner electrons were replaced by PAW frozen cores[24,30] while the valence monoelectronic states were expanded in plane waves with a kinetic cut-off energy of 450 eV. The metal slabs were constructed with 5 to 10 layers depending on the degree of openness of the (111), (100), (110), (211), and (520) surfaces, as shown in Figure 1. The structures were interleaved by 12 Å vacuum. In all cases optimizations were performed for the topmost half layers whereas the rest were kept constant to mimic the bulk. The corresponding k-point samplings were denser than 0.3 Å^{-1}. The dipole correction was employed to correct potential spurious terms arising from the asymmetry of the slabs.[31] With such a set up our surface energies were found to converge up to 0.005 eV/Å^2. The calculation details and benchmarks are presented in the Supporting Information (SI, in Figure SI-1and Table SI-1). The calculated surface energies are similar to others previously reported in the literature with DFT.[25,32-37] Experimental surface energies have only been reported for the lowest energy facet (111) and are quite scattered, values range from 1.54 J/m^2 to 1.1 J/m^2.[38,39] The equilibrium morphology of the nanoparticles is obtained through the Wulff construction method,[40] which depends on the relative surface energies (Table SI-2). Therefore, systematic deviations between calculated and experimental surface energies do not affect the reconstructed nanoparticle shape.[25,41] The crystal morphology model was created with the VESTA (Visualization for Electronic and STructural Analysis) version 3.1.4 package.[42] Adsorption was only allowed on one of the sides of the slab in the largest possible concentration as previously reported in ref.[43]. The adsorption energies of halide anions were derived from the Born-Haber cycle.[44]

The interaction of halogens, X, (or halides, X$^-$) on these surfaces was computed with respect to the neutral molecules (or the solvated ions). The adsorption energy of halogen atoms is similar in the case of Cl and Br and only slightly larger for I, due to its larger polarizability, see Figure 2. Halogen atoms prefer to adsorb at the defective positions of the surface; the extra stabilization gained at low-coordinated sites is quite small, 0.15 eV (much smaller than the value for CO, about 1 eV[45]). However, the adsorption of neutral halogen atoms cannot explain why Br is preferred in the synthetic process. If instead halide adsorption is inspected then the solvated ions are taken as the reference point. Solvation energies are larger for ions with small radii and thus Cl$^-$ is adsorbed more weakly than Br$^-$ and I$^-$, for which specific adsorption was described in electrochemical environments.[43] These results show that Cl$^-$ is endothermically adsorbed to the surface while Br$^-$ is almost thermoneutral, and I$^-$ is quite exothermically bonded. Therefore, overlayers of Cl$^-$ would be too labile to block surface growth due to rapid adsorption/desorption processes.[46] Therefore, equilibrium structures close to the Wulff construction are likely preferred when these atoms are present. On the contrary, I$^-$ is too strongly bound to the surface, thus blocking the growth process or the self-healing ability of sufficiently labile structures. In comparison, the specific adsorption of Br$^-$ species on the different surfaces is strong enough to structure the particle but weak enough to allow self-healing (adsorption/readsorption) during the growth process. This implies that halide adsorption can determine to a certain extent the preferred facets but cannot change the morphology of the seeds.

However, the interaction of the halides with the surface cannot explain two key factors in the structure of the nanorods. The most important is that NR growth from the spherical seed requires a symmetry breaking event that induces the preferential growth in one particular direction. A second aspect that requires investigation is that the lateral facets are high index planes

preferentially identified as {520}. Therefore, a detailed analysis on the initial growth step is required.
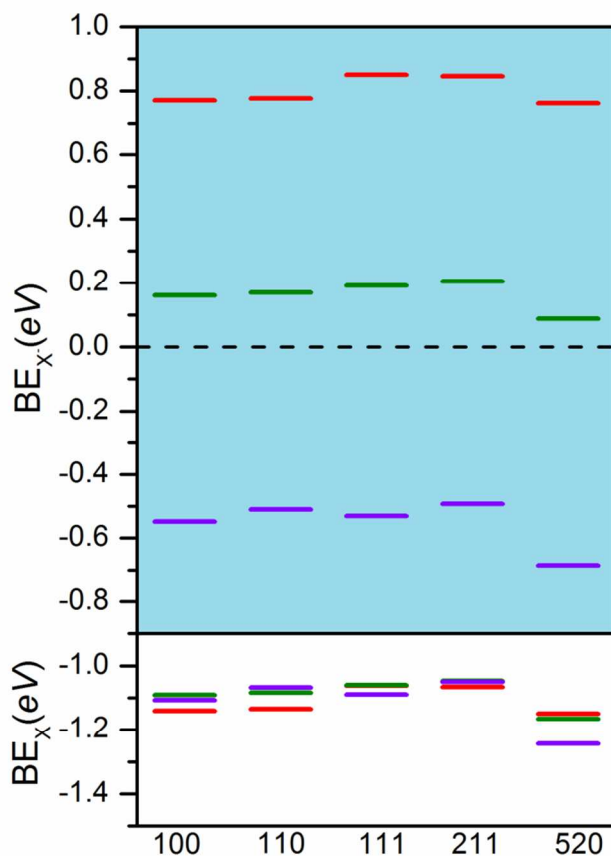

Figure 2. Binding energy of atomic halogen series to the different Au surfaces with respect to the X_2 molecule and for the solvated halide anions X^- (X and X^-; Cl = red, Br = olive and I =blue). It can be seen that while the values for the neutral species are constant, those of the ions differ significantly.

The structure of the small Au seeds can be estimated through Wulff construction with energies obtained from Figure 2, which leads to a cuboctahedron structure. The crystal morphologies of the Au nanoparticle are shown in Figure 3; the main surface is formed by {111} planes with small contributions from {100}. The structures are in good agreement with earlier experimental

and theoretical results.[25,41] Vaia *et al.* suggested that this is the stage at which the 1-2 nm seed is

completed. The seed is therefore associated with some adsorbed Br atoms, but is not in contact

with the CTA^+ micelle as the radius of the latter is larger at about 2.6 nm.[15]
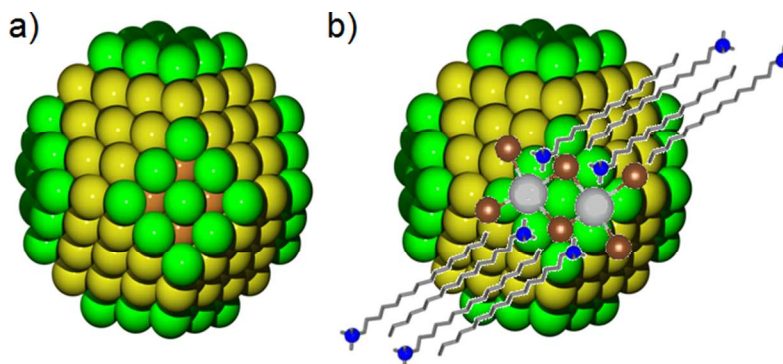
Figure 3. (a) Wulff construction of a gold nanoparticle representative of the seed. Yellow planes

are {111} and green ones are {100} facets. (b) The adsorption of CTAB-AgBr on {100} planes.

Note that due to the competition between electrostatic and chain interactions it is impossible to

cover all six {100} facets and thus a cylindrical configuration is templated during growth.

   The seeds enclosed in the soft-template of the micelle that resemble those in Figure 3(a) are

then added to the growth mixture which contains $AgNO_3$, more CTA^+, Br^-, and the mild reducing

agent controlled by solution pH. Growth starts by diffusion of the gold atoms into the CTA^+

micelle cavity.[47] Ag^+ is needed to ensure a 100% yield of nanorods, therefore it should induce

symmetry breaking, but its precise role has not been fully discerned. We calculated the

adsorption of Ag on the different gold facets. As previously identified in ref. [20], adsorption

preferentially takes place on open facets, but the energy gain between {111} and {110} is only

0.33 eV, not enough to ensure the appearance of open facets and most importantly, it cannot

justify anisotropy.

To understand the synergetic roles of the different chemical species in the growth solution we

started by optimizing the crystal structure of CTAB (Figure 4(a)), in which the stacking of the

aliphatic tails and the electrostatic interactions between the charged ammonium head groups and

Br^- become clear. However, in the growth solution Ag^+ cations and Br^- anions are present. The

formation of $[Br-Ag-Br]^-$ complexes is exothermic by 2.4 eV in agreement with the $[Br-Ag-Br]^-$

complexes identified on gold surfaces.[9] These complexes that can be entrapped by the CTA^+

cations forming the crystal presented in Figure 4(b). AgBr intercalation in the CTAB lattice

implies an energy gain of -0.70 eV/AgBr unit. In this structure the van der Waals interactions

between tails remain and the ionic interaction takes place between intact ammonium and [Br-Ag-

Br]$^-$, hereafter identified as CTAB-AgBr.[48] These intercalation compounds have been previously

proposed by Hubert *et al.* as responsible for symmetry breaking and nanorod growth.[49]
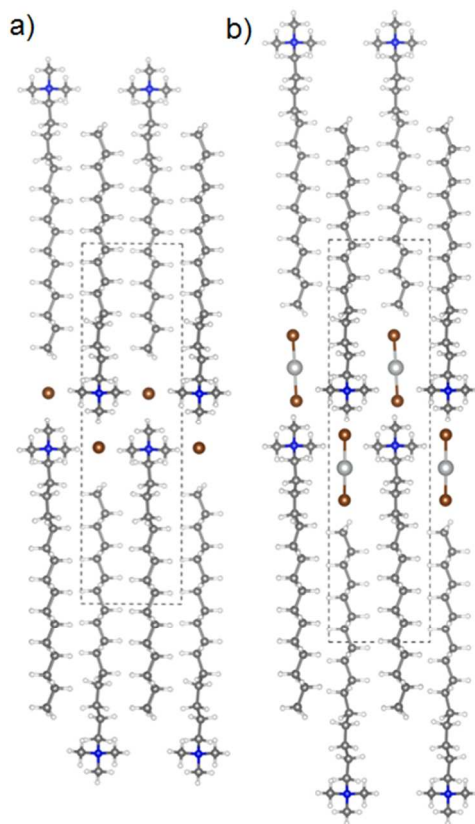
Figure 4. Crystal lattices of (a) CTAB and (b) CTAB-AgBr. (Br in brown, Ag as large light grey spheres, C grey, H white, N in blue).

Now, in the growth solution the gold seeds exhibiting {111} and {100} surfaces are placed in contact with CTAB-AgBr. Due to the geometric structure the {100} facets can allow the adsorption of the CTAB-AgBr as shown in Figure 3(b). The energy gain by adsorption of CTAB-AgBr is larger than 3 eV/CTAB-AgBr per molecule. The reason for the preferential adsorption on {100} is that CTAB-AgBr is preserved upon adsorption and patches of the AgBr crystal can epitaxially grow on the {100} facet of the original seed. Simultaneously, the structure keeps the aliphatic interactions between the tails while allowing the electrostatic bonding between Br$^-$ and ammonium cations. This type of adsorption cannot be retrieved for the {111}

facets as the AgBr crystal shows a rock-salt structure with non-polar planes of square patterns with good registry with the Au{100} surface. This preferential adsorption with subsequent blocking might easily be the origin of symmetry breaking and rod formation. Indeed, the structure of the nanoparticle is such that at most four out of the six {100} surfaces can be simultaneously covered by CTAB-AgBr. It shall be noticed that the small area of Ag^+ or [Br-Ag-Br]$^-$ complexes would not be able to block only four out of the six surfaces in the cubocahedron. Thus the mechanism by which silver under-deposition causes oriented growth in ionic liquids might be more complex than initially suggested.[20] The surfaces that are blocked in this manner induce the growth in a direction perpendicular to them (a [100] direction, in agreement with that found experimentally). The observation above is in line with the different energy requirements that Grochola *et al.*[19] identified as compulsory to obtain symmetry breaking and nanorod formation. We have thus identified the atomistic structure responsible for the stronger interaction. The preferential adsorption on some of the {100} facets leads to the structure in Figure 3(b), in which the formation of a sort of tube due to the ionic interaction between Ag-Br, growth on the {100} surface, electrostatic interactions between CTA^+ and terminal Br$^-$, and the dispersion interactions between CTA^+ effectively hinder further growth of the structure except in the longitudinal [100] direction. As the surfactants have a long aliphatic chain they try to align to maximize attraction, effectively generating a funnel that sets a preferential growth direction, leading to a sheaf-like structure. This further supports that the symmetry breaking takes place at very early stages as identified by Vaia *et al.*[15] According to our calculations it is likely that the aspect ratio is controlled by the length of the aliphatic chain of the surfactant, something that shall certainly be the subject of further experimental studies.

Regarding the most stable structure after growth is completed, we calculated the relative energies of the various surfactant coated surfaces proposed in the literature: {100}; {110}; and {520}. {520} contains 2(110)+3(100), forming short and long terraces separated by steps, as shown in Figure 1. Starting with the specific adsorption sites of these facets it is possible to match the structures of the CTAB-AgBr crystal shown in Figure 4 with the different surfaces. Due to space restrictions, adsorption takes place perpendicular to the surface following the epitaxial growth suggested in ref. [17]. The energy changes related to the proposed final state (thermodynamics) of the different elementary steps that control the growth of the long lateral facets are displayed in Figure 5.

The CTAB-AgBr complex can be adsorbed on top of the gold surface, Step 1, and lose one of the Br atoms, Step 2 (CTAB-Ag separated from Br). This leaves an Ag atom on the gold surface still with a Br coordinated to it and with a CTA^+ capping it. The subsequent reaction (Step 3) comprises completion of the new facet with incoming Au atoms complexed to CTA that get reduced on the surface. The thermodynamic parameters shown in Figure 5 indicate that the {520} surface has a distribution that shows short and long terraces that can accommodate the tails and the heads of the surfactant respectively. The interaction with {110} and {100} surfaces is less effective, see Figure 5. The final state implies that the energy reduction of the {520} surface is much larger than that of the {100} and {110} facets. Vaia *et al.*[15] have shown that the high index lateral facets develop in the last stages of growth. This agrees well with our simulations as for small seed particles the positions of some of the {520} planes cannot fit in the dimensions of the nanostructure.[25]
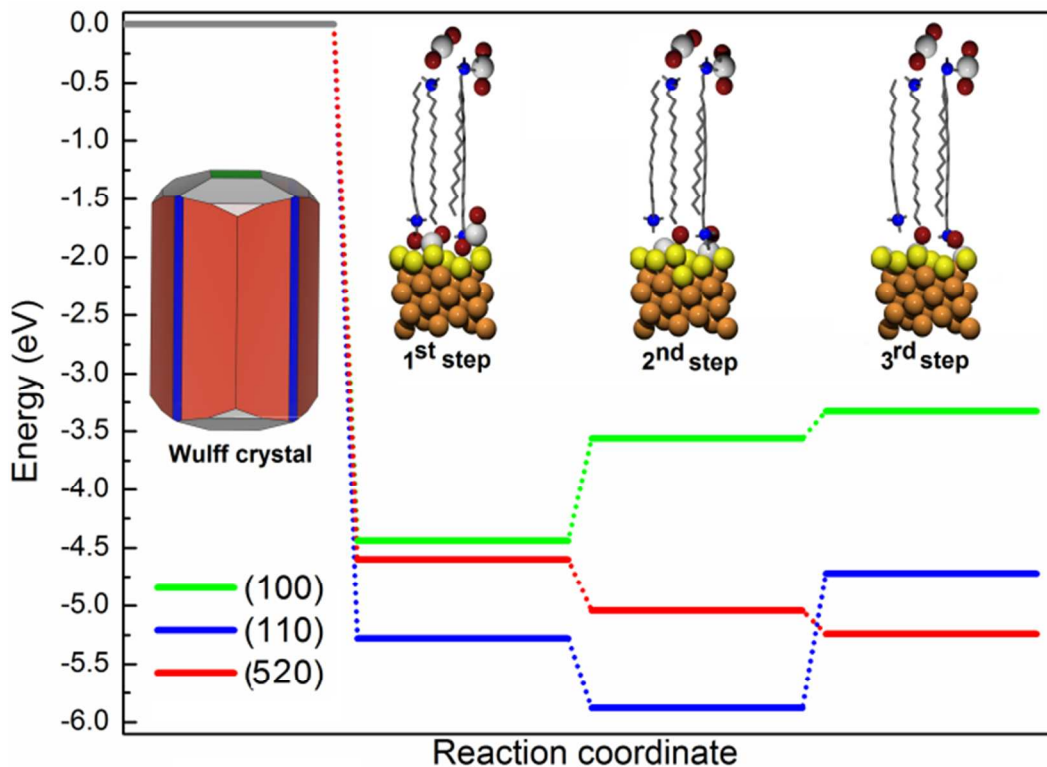
Figure 5. Incorporation and growth of a new Au layer onto a pre-existing structure for different surfaces. Step 1 corresponds to the surface adsorption of the CTAB-AgBr complex, Step 2 to the loose of one Br atom and Step 3 to the filling of resting positions in the lattice by Au atoms from the solution. Color code: yellow surface Au atoms, orange bulk Au, light grey Ag, brown Br, blue N, the aliphatic skeleton of the CTA^+ surfactant is shown as sticks. The inset shows the final Wulff structure upon CTAB adsorption showing {520} planes in red, as the most abundant lateral facets and {110} between them in navy.

With the calculated surface energies for the {100}, {110}, and {520} it is possible to simulate the nanorods by modifying the surface energies in the Wulff structure. The result is shown in Figure 5, as displayed in insets, clearly indicating that the {520} is the most common lateral surface and small terraces of {110} structure are also present. Thus the control of the final lateral

structures seems to be mainly of thermodynamic origin. Moreover, the {520} facets are the best at keeping the van der Waals interactions in the surfactant crystal structures. In contrast, for too small terraces it might be possible that the energy gained by surfactant stacking cannot revert the ordering of the original surface energies of the low-index {100} or {110} planes. Our results are important since we are able to provide a rational that can account for many of the results available from the experiments.

In summary, we have presented a model based on Density Functional Theory surface energy calculations to understand the leading interactions that drive the formation of gold nanorods through the well-known seeded growth method. The complexity of the procedure can be analyzed in detail by DFT simulations and the information provided by the calculations paves the way to a better understanding of synthetic-structure relationships.

ASSOCIATED CONTENT

Supporting Information. Calculation details and benchmarks; Table and Figure of (*i*) adsorption of X(X⁻) at gold surfaces; (*ii*) CTAB and CTAB-AgBr surfactants, including cif files for both; (*iii*) ascorbic acid adsorption, (*iv*) CTAB and CTAB-AgB on gold surfaces. This material is available free of charge via the Internet at http://pubs.acs.org.

AUTHOR INFORMATION

Corresponding Author

* Phone (+34) 977 920 237. Fax: (+34) 977 920 231. E-mail: nlopez@iciq.es Homepage:

http://www.iciq.es/portal/350/default.aspx

Author Contributions

Calculations were carried out by N.A.-B., G. N.-L. and P.W. The manuscript was written through contributions of all authors. All authors have given approval to the final version of the manuscript.

Notes

The authors declare no competing financial interest.

ACKNOWLEDGMENT

REFERENCES

(1)   Grzelczak, M.; Perez-Juste, J.; Mulvaney, P.; Liz-Marzan, L. M. *Chem. Soc. Rev.* **2008**, *37*, 1783-1791.
(2)   Dreaden, E. C.; Alkilany, A. M.; Huang, X. H.; Murphy, C. J.; El-Sayed, M. A. *Chem. Soc. Rev.* **2012**, *41*, 2740-2779.
(3)   Lohse, S. E.; Murphy, C. J. *Chem. Mat.* **2013**, *25*, 1250-1261.
(4)   Jain, P. K.; Huang, X. H.; El-Sayed, I. H.; El-Sayed, M. A. *Accounts Chem. Res.* **2008**, *41*, 1578-1586.
(5)   Perez-Juste, J.; Pastoriza-Santos, I.; Liz-Marzan, L. M.; Mulvaney, P. *Coord. Chem. Rev.* **2005**, *249*, 1870-1901.
(6)   Eustis, S.; El-Sayed, M. A. *Chem. Soc. Rev.* **2006**, *35*, 209-217.

(7)   Murphy, C. J.; San, T. K.; Gole, A. M.; Orendorff, C. J.; Gao, J. X.; Gou, L.; Hunyadi, S. E.; Li, T. *J. Phys. Chem. B* **2005**, *109*, 13857-13870.

(8)   Grzelczak, M.; Sanchez-Iglesias, A.; Rodriguez-Gonzalez, B.; Alvarez-Puebla, R.; Perez-Juste, J.; Liz-Marzan, L. M. *Adv. Funct. Mater.* **2008**, *18*, 3780-3786.

(9)   Niidome, Y.; Nakamura, Y.; Honda, K.; Akiyama, Y.; Nishioka, K.; Kawasaki, H.; Nakashima, N. *Chem. Comm.* **2009**, 1754-1756.

(10)   Gomez-Grana, S.; Hubert, F.; Testard, F.; Guerrero-Martinez, A.; Grillo, I.; Liz-Marzan, L. M.; Spalla, O. *Langmuir* **2012**, *28*, 1453-1459.

(11)   Wang, Z. L.; Mohamed, M. B.; Link, S.; El-Sayed, M. A. *Surf. Sci.* **1999**, *440*, L809-L814.

(12)   Katz-Boon, H.; Rossouw, C. J.; Weyland, M.; Funston, A. M.; Mulvaney, P.; Etheridge, J. *Nano Lett.* **2011**, *11*, 273-278.

(13)   Carbo-Argibay, E.; Rodriguez-Gonzalez, B.; Gomez-Grana, S.; Guerrero-Martinez, A.; Pastoriza-Santos, I.; Perez-Juste, J.; Liz-Marzan, L. M. *Angew. Chem.-Int. Edit.* **2010**, *49*, 9397-9400.

(14)   Goris, B.; Bals, S.; Van den Broek, W.; Carbo-Argibay, E.; Gomez-Grana, S.; Liz-Marzan, L. M.; Van Tendeloo, G. *Nat. Mater.* **2012**, *11*, 930-935.

(15)   Park, K.; Drummy, L. F.; Wadams, R. C.; Koerner, H.; Nepal, D.; Fabris, L.; Vaia, R. A. *Chem. Mat.* **2013**, *25*, 555-563.

(16)   Feng, J.; Slocik, J. M.; Sarikaya, M.; Naik, R. R.; Farmer, B. L.; Heinz, H. *Small* **2012**, *8*, 1049-1059.

(17)   Feng, J.; Pandey, R. B.; Berry, R. J.; Farmer, B. L.; Naik, R. R.; Heinz, H. *Soft Matter* **2011**, *7*, 2113-2120.

(18)   Heinz, H.; Farmer, B. L.; Pandey, R. B.; Slocik, J. M.; Patnaik, S. S.; Pachter, R.; Naik, R. R. *J. Am. Chem. Soc.* **2009**, *131*, 9704-9714.

(19)   Grochola, G.; Snook, I. K.; Russo, S. P. *J. Chem. Phys.* **2007**, *127*, 194707.

(20)   Jha, K. C.; Liu, H.; Bockstaller, M. R.; Heinz, H. *J. Phys. Chem. C* **2013**, 25969–25981.

(21)   Norskov, J. K.; Bligaard, T.; Rossmeisl, J.; Christensen, C. H. *Nature Chemistry* **2009**, *1*, 37-46.

(22)   Kresse, G.; Furthmuller, J. *Phys. Rev. B* **1996**, *54*, 11169-11186.

(23)   Kresse, G.; Furthmuller, J. *Comput. Mater. Sci.* **1996**, *6*, 15-50.

(24)   Kresse, G.; Joubert, D. *Phys. Rev. B* **1999**, *59*, 1758-1775.

(25)   Barmparis, G. D.; Remediakis, I. N. *Phys. Rev. B* **2012**, *86*, 085457.

(26)   Perdew, J. P.; Burke, K.; Ernzerhof, M. *Phys. Rev. Lett.* **1996**, *77*, 3865-3868.

(27)   Grimme, S. *J. Comput. Chem.* **2006**, *27*, 1787-1799.

(28)   Grimme, S.; Antony, J.; Ehrlich, S.; Krieg, H. *J. Chem. Phys.* **2010**, *132*, 154104.

(29)   Ruiz, V. G.; Liu, W.; Zojer, E.; Scheffler, M.; Tkatchenko, A. *Phys. Rev. Lett.* **2012**, *108*, 146103.

(30)   Bucko, T.; Hafner, J.; Lebegue, S.; Angyan, J. G. *J. Phys. Chem. A* **2010**, *114*, 11814-11824.

(31)   Neugebauer, J.; Scheffler, M. *Phys. Rev. B* **1992**, *46*, 16067-16080.

(32)   Vitos, L.; Ruban, A. V.; Skriver, H. L.; Kollar, J. *Surf. Sci.* **1998**, *411*, 186-202.

(33)   Galanakis, I.; Bihlmayer, G.; Bellini, V.; Papanikolaou, N.; Zeller, R.; Blugel, S.; Dederichs, P. H. *Europhys. Lett.* **2002**, *58*, 751-757.

(34)   Singh-Miller, N. E.; Marzari, N. *Phys. Rev. B* **2009**, *80*, 235407.

(35)   Shi, H.; Stampfl, C. *Phys. Rev. B* **2008**, *77*, 094127.

(36)   Gomez-Grana, S.; Goris, B.; Altantzis, T.; Fernandez-Lopez, C.; Carbo-Argibay, E.; Guerrero-Martinez, A.; Almora-Barrios, N.; Lopez, N.; Pastoriza-Santos, I.; Perez-Juste, J.; Bals, S.; Van Tendeloo, G.; Liz-Marzan, L. M. *J. Phys. Chem. Lett.* **2013**, *4*, 2209-2216.

(37)   Wen, Y.-N.; Zhang, H.-M. *Solid State Commun.* **2007**, *144*, 163-167.

(38)   Tyson, W. R.; Miller, W. A. *Surf. Sci.* **1977**, *62*, 267-276.

(39)   Ricci, E.; Novakovic, R. *Gold Bull.* **2001**, *34*, 41-49.

(40)   Wulff, G. *Z Krystallogr. Mineral* **1901**, *34*, 449-530.

(41)   Cleveland, C. L.; Landman, U.; Shafigullin, M. N.; Stephens, P. W.; Whetten, R. L. *Z. Phys. D-Atoms Mol. Clusters* **1997**, *40*, 503-508.

(42)   Momma, K.; Izumi, F. *J. Appl. Crystallogr.* **2011**, *44*, 1272-1276.

(43)   Magnussen, O. M. *Chem. Rev.* **2002**, *102*, 679-725.

(44)   Gomez-Diaz, J.; Honkala, K.; Lopez, N. *Surf. Sci.* **2010**, *604*, 1552-1557.

(45)   Lopez, N.; Nørskov, J. K. *J. Am. Chem. Soc.* **2002**, *124*, 11262-11263.

(46)   The possible effect of ascorbic acid as capping agent is presented in the Supporting Information Section "Adsorption of ascorbic acid on Au surface"

(47)   Nikoobakht, B.; El-Sayed, M. A. *Chem. Mat.* **2003**, *15*, 1957-1962.

(48)   Liu, X. H.; Luo, X. H.; Lu, S. X.; Zhang, J. C.; Cao, W. L. *J. Colloid Interf. Sci.* **2007**, *307*, 94-100.

(49)   Hubert, F.; Testard, F.; Spalla, O. *Langmuir* **2008**, *24*, 9219-9222.

FIGURE_TOC